JOURNAL OF COMPUTATIONAL PHYSICS **140,** 233–258 (1998)
ARTICLE NO. CP975882

Generation of Turbulent Inflow Data for Spatially-Developing Boundary Layer Simulations

Thomas S. Lund*

Center for Turbulence Research, Stanford University, Stanford, California 94305
E-mail: lund@utacfd.uta.edu

and

Xiaohua Wu and Kyle D. Squires

Department of Mechanical and Aerospace Engineering, Arizona State University, Tempe, Arizona 85287-6106

Received June 20, 1996

A method for generating three-dimensional, time-dependent turbulent inflow data for simulations of complex spatially developing boundary layers is described. The approach is to extract instantaneous planes of velocity data from an auxiliary simulation of a zero pressure gradient boundary layer. The auxiliary simulation is also spatially developing, but generates its own inflow conditions through a sequence of operations where the velocity field at a downstream station is rescaled and re-introduced at the inlet. This procedure is essentially a variant of the Spalart method, optimized so that an existing inflow–outflow code can be converted to an inflow-generation device through the addition of one simple subroutine. The proposed method is shown to produce a realistic turbulent boundary layer which yields statistics that are in good agreement with both experimental data and results from direct simulations. The method is used to provide inflow conditions for a large eddy simulation (LES) of a spatially evolving boundary layer spanning a momentum thickness Reynolds number interval of 1530–2150. The results from the LES calculation are compared with those from other simulations that make use of more approximate inflow conditions. When compared with the approximate inflow generation techniques, the proposed method is shown to be highly accurate, with little or no adjustment of the solution near the inlet boundary. In contrast, the other methods surveyed produce a transient near the inlet that persists several boundary layer thicknesses downstream. Lack of a transient when using the proposed method is significant since the adverse

* Present address: University of Texas at Arlington, Department of Mechanical and Aerospace Engineering, Box 19018, Arlington, TX 76019-0018.

0021-9991/98 $25.00

effects of inflow errors are typically minimized through a costly upstream elongation of the mesh. Extension of the method for non-zero pressure gradients is also discussed.

1. INTRODUCTION

Spatially evolving turbulent flows pose a particular challenge to numerical simulation approaches due to the need to prescribe time-dependent turbulent inflow conditions at the upstream boundary. In most cases the flow downstream is highly dependent on the conditions at the inlet, making it necessary to specify a realistic time series of turbulent fluctuations that are in equilibrium with the mean flow. This requirement often dictates that the inflow data should satisfy the Navier–Stokes equations, which in turn implies that an independent simulation be used to generate them. Detailed simulations for the purpose of creating inflow conditions can be costly and thus certain levels of approximation are desirable. In this paper we shall focus on an approximate yet accurate method for generating inflow conditions for spatially developing turbulent boundary layer simulations. The proposed method is essentially a simplification of the method of Spalart and Leonard [2], who devised an ingenious transformation that allows for the calculation of spatially evolving boundary layers in conjunction with periodic boundary conditions applied in the streamwise direction. While this method is elegant and highly accurate, it is more complicated than is necessary for the purpose of generating inflow data. A few key approximations are used in this work to arrive at a "modified Spalart method" that is very easy to implement and efficient to use. The new method is shown to yield results that compare well with the computations of Spalart [1]. It is also shown to produce very accurate inflow data while requiring only a small computational overhead.

2. SURVEY OF EXISTING INFLOW GENERATION TECHNIQUES

In order to justify our approach more fully, we first survey several of the existing turbulent inflow generation techniques and comment on their shortcomings. Perhaps the most straightforward approach to simulate a spatially developing turbulent boundary is to start the calculation far upstream with a laminar profile plus some random disturbances and then allow a natural transition to turbulence to occur. This approach has been used in simulations focusing on the transition process itself [3] and has the advantage that no turbulent fluctuations are required at the inlet. The procedure is not generally applicable to turbulent simulations, since, simulating the transition process is in itself a very costly venture and coupling this with a complex simulation for the downstream flow would be prohibitively expensive.

In order to reduce the cost associated with simulation of the transition process, most spatially evolving simulations start with an inflow boundary that is displaced only a short distance upstream of the region of interest. Ideally, one would like to provide sufficiently accurate inflow conditions at this boundary so that a realistic turbulent boundary layer with the correct skin friction and integral thicknesses is achieved within a short distance downstream. In practice, this is not always possible and the inflow boundary may have to be displaced further upstream in order to allow for relaxation of the errors made in approximating the inflow conditions. The inclusion of such a "development section" adds

to the overall cost of the simulation and therefore one would like to minimize its extent. At the same time, one would like to minimize the cost associated with generating the inflow data themselves. Unfortunately, these are conflicting requirements as simpler inflow generation techniques typically contain more error and therefore require a longer development section.

The simplest procedure for specifying turbulent inflow conditions is to superpose random fluctuations on a desired mean velocity profile. The amplitude of the random fluctuations can be constrained to satisfy a desired set of one-point, second-order statistics (i.e., Reynolds stress tensor). It is much more difficult to specify phase relationships between the velocity fluctuations, however, and these are invariably generated at random. Without proper phase information higher order correlations are incorrect and the flow lacks realistic turbulent structure. In addition, the velocity derivative skewness is zero and thus the inflow condition is void of nonlinear energy transfer. While synthetic turbulent fluctuations are easy to generate with the random method, a fairly lengthy development section must be used in order to allow for the development of organized turbulent motion.

Despite its shortcomings, the random fluctuation approach has been used with varying degrees of success. Lee *et al.* [4] used the approach for direct numerical simulation (DNS) of compressible isotropic turbulence, with and without the presence of a normal shock wave. They found that isotropic turbulence develops relatively quickly out of the random fluctuations and that the correct velocity derivative skewness was achieved after about two integral length scales of streamwise evolution. Rai and Moin [3] used a similar method to produce isotropic free-stream disturbances in DNS of the laminar-turbulent transition in a spatially developing boundary layer. Le and Moin [5, 6] extended this procedure to generate anisotropic turbulence and used the method to produce inflow fluctuations for DNS of a backward-facing step. Although a development section of 10 boundary layer thicknesses was used due to cost constraints, separate tests on a spatially evolving channel flow indicated that nearly 20 boundary layer thicknesses were required to recover the correct skin friction. Evidently the drastic changes to the flow caused by the massive separation overshadowed any residual errors in the quality of the turbulent boundary layer upstream of the step. Akselvoll and Moin [7, 8] attempted to use the same inflow method for their repeat of the backward-facing step using large eddy simulation (LES). Compared to Le and Moin [5, 6], they found that the random fluctuations did not develop nearly as rapidly on the coarser LES mesh. They opted to extract a time series of inflow data from a separate boundary layer calculation that made use of the random fluctuation method on a mesh that was refined in the spanwise and wall-normal directions. The streamwise extent for the inflow calculation was 25 boundary layer thicknesses. Good results for the flow downstream were obtained by supplying the velocity time series at the inflow boundary located 0.3 boundary layer thicknesses upstream of the step.

While the random fluctuation method has the obvious disadvantage that it requires a lengthy and therefore costly development section, it has a second, perhaps more serious, problem in that it is very hard to control the skin friction and integral thicknesses at the end of the development section (where one would really like to specify them). This difficulty is due to the fact that the transient which takes place in the development section is non-physical and therefore the evolution of the various boundary layer characteristics is not well described by standard empirical relations. Thus, it is extremely difficult to guess the upstream values of skin friction, momentum thickness, etc., so that these parameters evolve to the desired values by the end of the development section. This problem was one of the motivating factors that led Akselvoll and Moin [7, 8] to split the inflow calculation

into a separate simulation. By doing this, they were able to run the inflow simulation until it was stationary and then to choose a downstream station from which to extract inflow data, where the skin friction and boundary layer thickness were fairly close to the target values. Even after doing this, however, they were unable to simultaneously match both the skin friction and boundary layer thickness. They opted to favor the boundary layer thickness, which resulted in an underprediction of the skin friction by roughly 20%.

The procedure of Akselvoll and Moin [7, 8] is part of a more general class of methods whereby inflow boundary conditions are extracted from a dedicated auxiliary simulation. In these approaches, an "inflow generation" calculation is synchronized with the main simulation. At each time step, the velocity field on a plane at a fixed streamwise location is extracted from the inflow calculation and transferred to the inlet boundary of the main simulation.Various levels of approximation can be made in the inflow simulations and even the crudest of these will, in general, be more accurate than the random fluctuation method.

While running an auxiliary simulation to generate inflow data might seem prohibitively expensive, this is not necessarily the case. As we shall see, the use of actual simulation data for an inlet condition allows the development section to be either reduced or eliminated altogether. The cost savings due to a reduction in the development length will more than offset the cost of the auxiliary simulation in most cases.

The simplest auxiliary simulation approach for wall-bounded flows is to extract the velocity field from a separate simulation of a fully developed "parallel flow" in which periodic boundary conditions are imposed in both the streamwise and spanwise directions. This approach is ideally suited to internal flows subjected to a nonuniformity such as a diffuser, curve, or sudden expansion. Periodic boundary conditions are appropriate for fully developed flow, and inflow data extracted from such a calculation can be introduced to a spatially evolving simulation without need for a development section. This approach was used by Kaltenbach [9], where a periodic channel flow simulation was used to generate inflow conditions for LES of a plane diffuser.

A similar approach can be used to generate inflow conditions for spatially developing boundary layers. Again, periodic boundary conditions are used in the streamwise and spanwise directions, but a symmetry condition (vanishing vertical derivatives of the streamwise and spanwise velocity components, as well as vanishing vertical velocity) at the upper "wall" results in a boundary layer-like mean profile. This approach is economical and has the advantage that the inflow turbulence is fully developed. On the other hand, a parallel-flow boundary layer has no mean advection. When used as an inflow condition, a development section will be needed to establish the correct boundary layer spatial growth characteristics. The parallel-flow boundary layer method was used by Lund [10] and Lund and Moin [11] to generate inflow for LES of a boundary layer on a concave wall. A development section of 10 boundary layer thicknesses was found to be sufficient to contain the adjustment region and good results were obtained downstream of this position.

Accounting for spatial growth in the inflow condition requires a more sophisticated approach than those outlined above. Spalart [1] developed a clever method to account for spatial growth in simulations with periodic boundary conditions by adding source terms to the Navier–Stokes equations (see also Spalart and Leonard [2]). This method should be ideal for the task of inflow generation since it is capable of producing an equilibrium spatially evolving boundary layer, with direct control of the skin friction and momentum thickness. Despite its apparent advantages, there have been few attempts to use Spalart's method for

the purpose of inflow generation. Na and Moin [12] used a somewhat related procedure to generate inflow data for DNS of attached and separated boundary layers. Instead of advancing the simulation in time, they attempted to save cost by using Taylor's hypothesis in conjuction with a single realization of Spalart's [1] velocity field to generate an approximate time series. Amplitudes of the velocity fluctuations were modulated randomly in time in an attempt to minimize the temporal periodicity inherited from application of Taylor's hypothesis to a spatially periodic domain. This method proved to be usable, although a development section of more than 10 boundary layer thicknesses was required to relax the errors associated with use of Taylor's hypothesis in a strongly sheared flow. Lund and Moin [11] advanced a Spalart-like simulation in time to generate inflow data for their simulation of a boundary layer of a concave wall. They observed almost no transient downstream of the inlet when this method was used.

3. TURBULENT INFLOW GENERATION METHOD

Based on our survey, it appears that a Spalart-type simulation run synchronously with the main simulation produces the most accurate inflow condition and provides the best control of the skin friction and momentum thickness. The only problem with the original Spalart method is that it is somewhat complicated to understand and to program. As explained below, the complications arise out of the need to introduce a coordinate transformation that minimizes the streamwise inhomogeneity. The resulting transformed equations require a special-purpose flow solver, as well as external inputs for the streamwise gradients of mean flow variables. While these complications are necessary to arrive at a highly accurate alogorithm for DNS studies, simplifications can be made for the task of generating inflow data. In this work we shall focus on a "modified Spalart method" that does not apply a coordinate transformation to the Navier–Stokes equations. Without a coordinate transformation, our method can be cast in a Cartesian coordinate system and can therefore make use of a conventional flow solver. In fact, using our approach, an existing inflow–outflow code can be converted to an inflow generation device through the addition of one simple subroutine. The resulting algorithm is easy to understand and program and is very efficient from a numerical standpoint. As we shall demonstrate, the method generates highly accurate inflow data and gives complete control on the skin friction and momentum thickness. We shall also demonstrate that it results in a significant savings in computational cost since a development section is not needed.

3.1. *Review of Spalart's Original Method*

The basic idea behind the method of Spalart and Leonard [2] is to define a set of coordinate lines along which the streamwise inhomogeneity associated with the boundary layer growth is minimized. When the Navier–Stokes equations are transformed into this coordinate system the velocity field is approximately homogeneous in the streamwise direction and is thus amenable to periodic boundary conditions. The periodic boundary conditions allow for a "self-contained" simulation that does not require external inputs for the upstream and downstream boundaries. In addition, periodic boundary conditions allow for the use of a highly accurate Fourier representation of the velocity field in the streamwise direction. While the advantages of periodic boundary conditions are apparent, they come at the expense of a more complicated set of equations to solve. The coordinate transformation introduces new

terms to the Navier–Stokes equations that account for the inhomogeneity in the streamwise direction. These so-called "growth terms" are both numerous and complicated in form. Spalart was able to show that a few of the terms are of higher order and therefore could be neglected. Several terms still remain, however, and these involve streamwise gradients of the mean flow variables, which must be supplied externally. In his 1988 work, Spalart advocates deducing these quantities from two or more simulations performed at different Reynolds numbers.

3.2. *Proposed Modification to Spalart's Method*

The main disadvantage of Spalart's method is the need to evaluate the growth terms. The presence of these terms requires a special flow solver along with the possibility of having to perform multiple simulations in order to estimate streamwise gradients of the mean flow quantities. In this section we propose a modification of Spalart's method that effectively eliminates the need to deal with the growth terms. This is achieved by electing to transform only the boundary conditions, as opposed to the entire solution domain. In effect, the proposed method computes a spatially evolving boundary layer in a Cartesian coordinate system but makes use of the ideas of Spalart and Leonard [2] to create a quasi-periodic boundary condition in the streamwise direction. This approach has the advantage that an existing Cartesian inflow–outflow simulation code can be adapted for the purpose of inflow generation by straightforward modifications to the streamwise boundary conditions. Furthermore, the spatial development of the boundary layer is computed directly and only a single empirical relation is required to relate the wall shear at the inlet boundary to the solution downstream.

Our simplifications come at the expense of the loss of strict periodic boundary conditions in the streamwise direction and therefore the inability to use a Fourier representation.This is not a concern in the context of inflow generation, however, since the recipient spatially evolving simulation will invariably use discrete operators. There is little to be gained from generating inflow data with a numerical method that is significantly more accurate than the one used in the main simulation. In fact, our experience has been that nonphysical transients often arise near the inlet boundary when inflow data generated with a high fidelity method are subjected to the increased numerical errors associated with the use of lower order approximations in the inflow–outflow simulation.

The heart of our method is a means of estimating the velocity at the inlet plane, based on the solution downstream. In particular, we extract the velocity field from a plane near the domain exit, make use of the ideas of Spalart and Leonard [2] to rescale it, and then reintroduce it as a boundary condition at the inlet.[1] A conventional convective outflow boundary condition (described in more detail below) is applied at the exit boundary. In effect, this procedure results in a straightforward spatially evolving simulation that generates its own inflow data. Coding changes are minimal since the only required modification is a single subroutine used to rescale the velocity from the downstream station.

In order to arrive at our rescaling procedure, we follow Spalart and Leonard [2] who first decomposed the velocity into a mean and fluctuating part and then applied the appropriate

[1] Our approach has some vague similarities with the more elaborate method of Spalart and Watmuff [13] who add source terms to the Navier–Stokes equations in the "fringe" region in an attempt to reverse spatial development effects prior to reassigning the downstream velocity field to the inlet.

scaling laws to each component separately. The decomposition is achieved by defining the mean (denoted by upper case) as an average in the spanwise direction and in time. The velocity fluctuations are then defined as

$$u_i'(x, y, z, t) = u_i(x, y, z, t) - U_i(x, y). \tag{1}$$

In this work we shall denote the streamwise, wall-normal, and spanwise velocity components by u, v, and w, with the corresponding coordinates being x, y, and z.

The mean flow is rescaled according to the law of the wall in the inner region and the defect law in the outer region. The law of the wall reads

$$U^{\text{inner}} = u_\tau(x)\, f_1(y^+), \tag{2}$$

where $u_\tau = \sqrt{\nu(\partial u/\partial y)_{\text{wall}}}$ is the friction velocity, $y^+ = (u_\tau y)/\nu$ is the wall coordinate, and f_1 is a universal function to be determined. The defect law is

$$U_\infty - U^{\text{outer}} = u_\tau(x)\, f_2(\eta), \tag{3}$$

where $\eta = y/\delta$ is the outer coordinate (δ is the boundary layer thickness), U_∞ is the free-stream velocity, and f_2 is a second universal function to be determined. Let U_{recy} and U_{inlt} denote the mean velocity at the downstream station to be recycled, and at the inlet, respectively. The law of the wall, (2), and the defect law, (3), dictate that U_{recy} and U_{inlt} are related in the inner and outer regions via

$$U_{\text{inlt}}^{\text{inner}} = \gamma U_{\text{recy}}\left(y_{\text{inlt}}^+\right) \tag{4}$$

and

$$U_{\text{inlt}}^{\text{outer}} = \gamma U_{\text{recy}}(\eta_{\text{inlt}}) + (1 - \gamma)U_\infty, \tag{5}$$

where

$$\gamma = \left(\frac{u_{\tau,\text{inlt}}}{u_{\tau,\text{recy}}}\right). \tag{6}$$

The independent variables in (4) and (5), y_{inlt}^+ and η_{inlt}, are the inner and outer coordinates of the grid nodes at the inlet station. Thus, $U_{\text{recy}}(y_{\text{inlt}}^+)$ is the mean velocity at the recycle station, expressed as a function of y^+ and evaluated at the inner coordinate of the mesh at the inlet. This evaluation requires an interpolation since the inner coordinates for the grid nodes at the recycle and inlet stations will, in general, be different. A linear interpolation was found to be sufficiently accurate for this purpose. A similar interpolation is required for the outer coordinate.

The mean vertical velocity in the inner and outer regions is assumed to scale as

$$V^{\text{inner}} = U_\infty\, f_3(y^+) \tag{7}$$

and

$$V^{\text{outer}} = U_\infty\, f_4(\eta), \tag{8}$$

where f_3 and f_4 are assumed to be universal functions. These scalings are used as convenient

approximations; they are not not fully consistent with scaling of the mean velocity profile, which, through the continuity equation, requires $V \sim (\nu/u_\tau)\, du_\tau/dx$ in the inner region and $V \sim u_\tau\, d\delta/dx$ in the outer region. The above approximations are justified, however, since V itself is a small quantity and accounting for the streamwise variations in u_τ and δ would introduce higher order corrections. The correct scalings could be used nonetheless, but this approach would require specification of the derivatives du_τ/dx and $d\delta/dx$ at the inlet, as well as a modification of the vertical velocity boundary condition given in (25).

Applied between the recycle and inlet stations, the assumed scaling for the vertical velocity leads to

$$V_{\text{inlt}}^{\text{inner}} = V_{\text{recy}}\left(y_{\text{inlt}}^{+}\right) \tag{9}$$

and

$$V_{\text{inlt}}^{\text{outer}} = V_{\text{recy}}(\eta_{\text{inlt}}). \tag{10}$$

The spanwise velocity should be zero in the mean and, thus, no scaling relations are required.

The velocity fluctuations in the inner and outer regions are decomposed further to give

$$(u_i')^{\text{inner}} = u_\tau(x) g_i(x, y^+, z, t) \tag{11}$$

and

$$(u_i')^{\text{outer}} = u_\tau(x) h_i(x, \eta, z, t). \tag{12}$$

The purpose of this decomposition is to isolate the streamwise inhomogeneity through the explicit dependence on u_τ. The functions g_i and h_i are then approximately homogeneous in the streamwise direction and are, therefore, amenable to periodic boundary conditions. In Spalart and Leonard [2] and Spalart [1], periodic boundary conditions are assumed at this stage. The procedure here is different since we have elected to retain an inflow–outflow structure. The fundamental difference in the present approach is that the "periodic" condition provides only one-way coupling between the recycle station and the inlet. The velocity fluctuations at the downstream station will be related to those at the inlet using (11) and (12), but there is no downstream transfer of information from the inlet via boundary conditions. The convective outflow condition applied at the domain exit provides the necessary downstream boundary condition.

Assuming the functions g_i and h_i to be "periodic" the velocity fluctuations at the inlet are related to those at the recycle station via

$$(u_i')_{\text{inlt}}^{\text{inner}} = \gamma (u_i')_{\text{recy}}\left(y_{\text{inlt}}^{+}, z, t\right) \tag{13}$$

and

$$(u_i')_{\text{inlt}}^{\text{outer}} = \gamma (u_i')_{\text{recy}}(\eta_{\text{inlt}}, z, t). \tag{14}$$

Equations (4)–(6), (9), (10), (13), and (14) provide a means of rescaling the mean and fluctuating velocity for both the inner and outer regions of the boundary layer. A composite

profile that is approximately valid over the entire layer is obtained by forming a weighted average of the inner and outer profiles:

$$(u_i)_{\text{inlt}} = \left[(U_i)_{\text{inlt}}^{\text{inner}} + (u_i')_{\text{inlt}}^{\text{inner}}\right][1 - W(\eta_{\text{inlt}})] + \left[(U_i)_{\text{inlt}}^{\text{outer}} + (u_i')_{\text{inlt}}^{\text{outer}}\right] W(\eta_{\text{inlt}}). \quad (15)$$

The weighting function $W(\eta)$ is defined as

$$W(\eta) = \frac{1}{2}\left\{1 + \tanh\left[\frac{\alpha(\eta - b)}{(1-2b)\eta + b}\right] \Big/ \tanh(\alpha)\right\}, \quad (16)$$

where $\alpha = 4$ and $b = 0.2$. The weighting function is zero at $\eta = 0$, 0.5 at $\eta = b$, and unity at $\eta = 1$. The parameter α controls the width of the region over which the function transitions from 0 to 1. For $\alpha \to \infty$ the distribution becomes a step function centered at $\eta = b$. As $\alpha \to 0$ the transition is spread across the entire boundary layer. The values of α and b quoted above were determined through analysis of an independent spatially evolving boundary layer simulation. With the present choice of α and b, the weight will exceed unity slightly for positions beyond the boundary layer edge ($\eta > 1$). Thus the additional constraint $W = 1$ for $\eta > 1$ should be imposed if the weight is required beyond $\eta = 1$.

The rescaling operation requires the scaling parameters u_τ and δ both at the recycle station and at the inlet. These quantities can be determined from the mean velocity profile at the rescale station, but they must be specified at the inlet. It turns out that the problem is over-determined if both u_τ and δ are fixed independently at the inlet, and thus, an additional relation is needed to connect one of these parameters at the inlet to the solution on the interior. While several suitable relations exist, we have obtained the best results by fixing δ at the inlet computing u_τ via

$$u_{\tau,\text{inlt}} = u_{\tau,\text{resc}}\left(\frac{\theta_{\text{resc}}}{\theta_{\text{inlt}}}\right)^{1/[2(n-1)]}, \quad n = 5, \quad (17)$$

where θ is the momentum thickness. The above relation is similar to the Ludwig–Tillmann correlation [14] and can be derived from the standard power-law approximations $C_f \sim R_x^{-1/n}$, $\theta/x \sim R_x^{-1/n}$. In many cases it is more advantageous to control the inlet momentum thickness than the inlet boundary layer thickness. This can be done with a little extra effort by iteratively adjusting the inlet boundary layer thickness until the target inlet momentum thickness is achieved.

The time average used to compute the mean velocity field can be a simple running average when the flow is fully developed, but should be modified in order to exclude starting transients if the solution is initialized with a crude guess. A convenient way to eliminate the starting transients is to use an average with a weight that decreases exponentially backward in time. The following formula achieves this,

$$U^{n+1} = \frac{\Delta t}{T}\langle u^{n+1}\rangle_z + \left(1 - \frac{\Delta t}{T}\right) U^n, \quad (18)$$

where Δt is the computational time step, T is the characteristic time scale of the averaging interval, and $\langle\,\rangle_z$ denotes an average in the spanwise direction. When attempting to eliminate transients, the averaging interval should be rather short; $T = 10\delta/U_\infty$ was found to work well for this purpose. Once the flow equilibrates, the averaging interval must be increased.

We obtained the best results by running for a period of a few hundred inertial times (δ/U_∞) with $T \simeq 100\delta/U_\infty$ in order to stabilize the statistics and then switching to a simple running average ($T = T_0 + t - t_0$, where t is the current time in the simulation, t_0 is the time at which the running averaging was initiated, and T_0 is the value of the averaging interval used prior to t_0).

4. NUMERICAL METHOD

In this section we describe the numerical method that will be used to generate the test results in the subsequent section. We should emphasize that the inflow generation procedure puts very little restriction on the numerical method, and thus, techniques different from those described in this section could equally well be used. In addition, while the modified Spalart method is equally applicable to DNS and LES studies, we choose to work with LES test cases in this work.

The filtered incompressible continuity and Navier–Stokes equations are

$$\frac{\partial \bar{u}_j}{\partial x_j} = 0, \tag{19}$$

$$\frac{\partial \bar{u}_i}{\partial t} + \frac{\partial \bar{u}_i \bar{u}_j}{\partial x_j} = -\frac{1}{\rho}\frac{\partial \bar{p}}{\partial x_i} + \nu \frac{\partial^2 \bar{u}_i}{\partial x_j \partial x_j} - \frac{\partial \tau_{ij}}{\partial x_j}, \tag{20}$$

where $\overline{(\,)}$ denotes application of the spatial filter. The subgrid-scale (SGS) stress $\tau_{ij} = \overline{u_i u_j} - \bar{u}_i \bar{u}_j$, which appears in (20) is parameterized by an eddy viscosity model

$$\tau_{ij} - \frac{1}{3}\delta_{ij}\tau_{kk} = -2\nu_T \bar{S}_{ij} = -2C\bar{\Delta}^2 |\bar{S}| \bar{S}_{ij}, \tag{21}$$

where δ_{ij} is the Kronecker delta and $|\bar{S}| = \sqrt{2S_{ij}S_{ij}}$ is the magnitude of the resolved-scale strain rate tensor, $\bar{S}_{ij} = 1/2(\partial \bar{u}_i/\partial x_j + \partial \bar{u}_j/\partial x_i)$. The trace of the SGS stress, τ_{kk}, is not modeled but rather is added to the pressure term. Closure of the SGS stress τ_{ij} is obtained through specification of the model coefficient C appearing in (21).

Following Germano *et al.* [15] the model coefficient, C, is determined dynamically by considering a velocity field filtered at a scale twice as large as that corresponding to the primary filter. The unresolved stress associated with the "test filtered" field is denoted by T_{ij} and is related to the subgrid-scale stress via

$$L_{ij} = T_{ij} - \hat{\tau}_{ij}, \tag{22}$$

where $L_{ij} = \widehat{\bar{u}_i \bar{u}_j} - \hat{\bar{u}}_i \hat{\bar{u}}_j$ is a computable "Leonard term" and $\widehat{(\,)}$ denotes the test-filter operation. Test filtering is performed in the streamwise and spanwise directions using a tophat filter of width equal to two mesh spacings.

When (21) as well as an analogous model for T_{ij} are substituted in the above relation, an overdetermined system of five equations for C arises. A unique value for C can be determined through a least-squares minimization procedure [16, 17]. The result is

$$2C\bar{\Delta}^2 = \frac{\langle L_{ij} M_{ij} \rangle_z}{\langle M_{kl} M_{kl} \rangle_z}, \tag{23}$$

where

$$M_{ij} = 4|\widehat{\bar{S}}|\widehat{\bar{S}}_{ij} - \widehat{|\bar{S}|\bar{S}_{ij}} \tag{24}$$

and where $\langle\,\rangle_z$ denotes an average in the spanwise direction. Other variants of the model are possible and the interested reader is referred to Ghosal *et al.* [17] and Meneveau *et al.* [18] for further discussion.

The numerical approach employed for the solution of (19) and (20) is the fractional step method (e.g., see Chorin [19], Kim and Moin [20]). Spatial derivatives are discretized using second-order central differences on a staggered mesh as proposed by Harlow and Welch [21]. The discrete system is time advanced in a semi-implicit fashion, where all terms with gradients in the wall-normal direction are treated implicitly with the Crank–Nicholson method while the remaining terms are treated explicitly with a third-order Runge–Kutta scheme.

The boundary conditions on the top surface of the computational domain are

$$\frac{\partial \bar{u}}{\partial y} = 0, \quad \bar{v} = U_\infty \frac{d\delta^*}{dx}, \quad \frac{\partial \bar{w}}{\partial y} = 0, \tag{25}$$

where δ^* is the boundary layer displacement thickness and U_∞ is the free-stream velocity. The derivative $d\delta^*/dx$ is computed from the mean velocity field by first computing δ^* as a function of x and then performing a linear regression on the resulting distribution to determine the average slope. Although local values of the slope could be used, $d\delta^*/dx$ is nearly constant over the limited Reynolds number variation in the present computations and little improvement is expected if a variable velocity distribution is used. It should be remarked, however, that local values of vertical velocity must be used if the method is applied to flows with nonzero pressure gradients. A short discussion of this point is included in the conclusions.

At the exit plane a convective boundary condition of the form $\partial \bar{u}_i/\partial t + c\partial \bar{u}_i/\partial x = 0$ is applied (c is the local bulk velocity; Han *et al.* [22]). The convective condition is augmented with a correction on the streamwise velocity to ensure global mass conservation. This operation is necessary since small changes in the mass flow through the inlet or upper boundaries can occur from time step to time step. The correction is implemented by multiplying the streamwise velocity on the exit plane by a spatially uniform scaling factor. The correction is typically on the order of 0.05%.

5. RESULTS

In order to validate our modifications to Spalart method, we first simulate a flat plate boundary layer spanning a momentum thickness Reynolds number range of $R_\theta = 1400$–1640 and compare the results with those of Spalart at $R_\theta = 1410$ and with Rai and Moin [3] at $R_\theta = 1350$. Next, a time series of velocity information at the midplane of this simulation is used to generate inflow conditions for a spatially evolving flat plate simulation covering a Reynolds number range of $R_\theta = 1530$–2150. Due to the fact that the inflow data is extracted from the central plane of inflow generation simulation, the two domains overlap as depicted in Fig. 1. This feature provides a critical test for the inflow generation technique; the results should be nearly identical in the region of overlap, and no changes in the streamwise evolution of boundary layer statistics should occur as the flow develops further downstream.

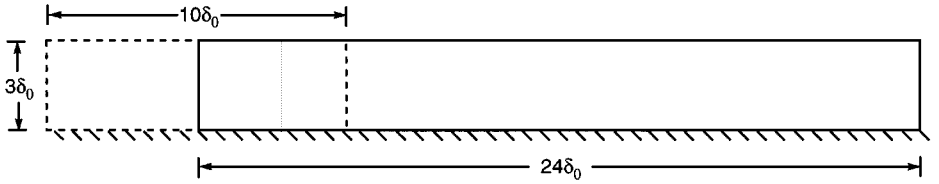

FIG. 1. Arrangement of the computational domains. The solid lines represent the boundaries of the inflow–outflow simulation while the dashed lines represent the inflow generation calculation using the modified Spalart method. The dotted line denotes the location of the recycle station in the inflow calculation.

For comparison, we also perform spatially evolving simulations using both the random fluctuation and parallel flow methods.

5.1. *Inflow Generation Simulation*

The computational domain for the modified Spalart simulation is shown as the dashed curve in Fig. 1 and has dimensions $10\delta_0 \times 3\delta_0 \times (\pi/2)\delta_0$ in the streamwise, wall-normal, and spanwise directions, respectively, where δ_0 is the 99% boundary layer thickness at the midpoint of the domain. The momentum thickness Reynolds number at the inflow plane is fixed at $R_\theta = 1400$. The mesh contains $100 \times 45 \times 64$ points in the streamwise, wall-normal, and spanwise directions, respectively. In wall units (using the wall shear evaluated at the midpoint), the mesh resolution is $\Delta x^+ \approx 64$, $\Delta y^+_{\text{wall}} \approx 1.2$, and $\Delta z^+ \approx 15$. The mesh is uniform in the streamwise and spanwise directions while a hyperbolic tangent stretching is used in the normal direction to cluster points near the wall.

The recycle station was located $8.25\,\delta_0$ downstream of the inlet (dotted line in Fig. 1). The domain exit was not chosen as the recycle station in order to avoid transferring errors associated with the outflow boundary condition to the inlet via the rescaling operation. The station $8.25\,\delta$ was determined to be as far downstream as possible without being affected by outflow boundary condition errors.

The velocity field was initialized with the mean profile given by the Spalding [23] law. Random fluctuations with a maximum amplitude of 10% of the free-stream value were superimposed on the mean profile. The solution was advanced with a time step of roughly two viscous time units ($\Delta t \approx 2\nu/u_\tau^2$). The simulation was run initially for 1100 inertial timescales δ_0/U_∞ in order to eliminate starting transients. Statistics were then sampled over a period of 1400 inertial timescales. The results from this simulation will be plotted along with those from the spatially-evolving simulation and discussed in the following subsection.

5.2. *Spatially Evolving Simulation Using Turbulent Inflow*

The simulation discussed in the previous subsection was used to generate inflow conditions for an inflow–outflow calculation of a flat-plate boundary layer covering the Reynolds number range $R_\theta = 1530$–2150. The computational domain for this simulation is shown as the solid line in Fig. 1. It has the same wall-normal and spanwise dimensions ($3\delta_0 \times (\pi/2)\delta_0$) as the modified Spalart simulation, but it is nearly two and a half times as long in the streamwise direction ($24\,\delta_0$). The mesh spacings are identical in the two cases. The inflow–outflow calculation makes use of $240 \times 45 \times 64$ grid points.

In order to evaluate the accuracy of the inflow condition obtained using the modified Spalart method, calculations were also performed using the simpler random fluctuation and parallel-flow methods. These methods are described in more detail in Appendices A and B, respectively. The parallel-flow method also requires a separate simulation and this was performed using the same computational domain, spatial resolution, and time step as in the modified Spalart case. The inflow obtained using the random fluctuation method was prescribed to have the same mean profile and Reynolds stress tensor as those produced by the modified Spalart method. For reasons that will become apparent below, the simulation using the random fluctuation method was performed on a domain twice as long in the streamwise direction as compared to the other two calculations ($48\,\delta_0$ vs $24\,\delta_0$).

In the case of the modified Spalart method, the simulation discussed in the previous subsection was first run to a statistically stationary state. Next a time sequence of two-dimensional velocity fields was extracted from the central plane and written to disk. The inflow–outflow calculation used this information by reading one plane of inflow data per time step. An analogous procedure was used for the parallel-flow method. Inflow data were generated on the fly for the random fluctuation method.

For each of the three calculations, the computation was initialized by copying the first plane of inflow data throughout the entire domain while superimposing random disturbances with amplitude equal to 10% of the local mean streamwise velocity profile. Following the initialization, a period of 70 inertial time units (U_∞/δ_0), or equivalently 2.9 flow through times (U_∞/X_L), were used to eliminate starting transients. Statistics were then accumulated over a period of 1400 inertial time units.

Figure 2a shows the evolution of the boundary layer thickness. For reference, the results from the momentum integral estimate based on Cole's Law of the wake [24] (described in Appendix C) are also included. Focusing first on the modified Spalart simulation and its corresponding inflow–outflow descendent (filled circle and solid line, respectively), it is apparent that there is virtually no difference in the evolution of the boundary layer thickness between the two simulations in the region of overlap (from $R_\theta = 1530$ to 1640). Furthermore, the slope that is established in the inflow calculation is preserved in the main simulation well beyond the region of overlap. This observation indicates that the rescaling procedure used in the modified Spalart method results in natural equilibrium boundary layer. The results from both these simulations are in excellent agreement with the momentum integral estimate. This is partly due to the normalization used which forces the computation to agree with the theory at the inlet of the inflow–outflow simulation. The relevant comparison is therefore the slope of the curve which is also accurate.

Turning to the alternative inflow generation methods, it is clear that these do not work as well. The parallel-flow method produces a clear transient that extends to roughly $R_\theta = 1850$. From that point, the evolution is acceptable, with the slope matching the momentum integral estimate reasonably well. An offset is generated by the transient, however, and this causes the boundary layer thickness to be about 10% lower than would be expected for a given value of R_θ. The random fluctuation inflow yields the worst results with the boundary layer thickness never growing at the correct rate. As will be apparent in later figures, the "turbulence" supplied at the inlet in the simulation with random fluctuation inflow decays with streamwise distance up to a point where a "transition" takes place and realistic turbulence begins to develop. This transition occurs between $R_\theta = 1600$ and 1700 and is responsible for the change in slope of the boundary layer thickness. The transition is not fully complete by the domain exit, however, and the correct growth rate is never achieved.

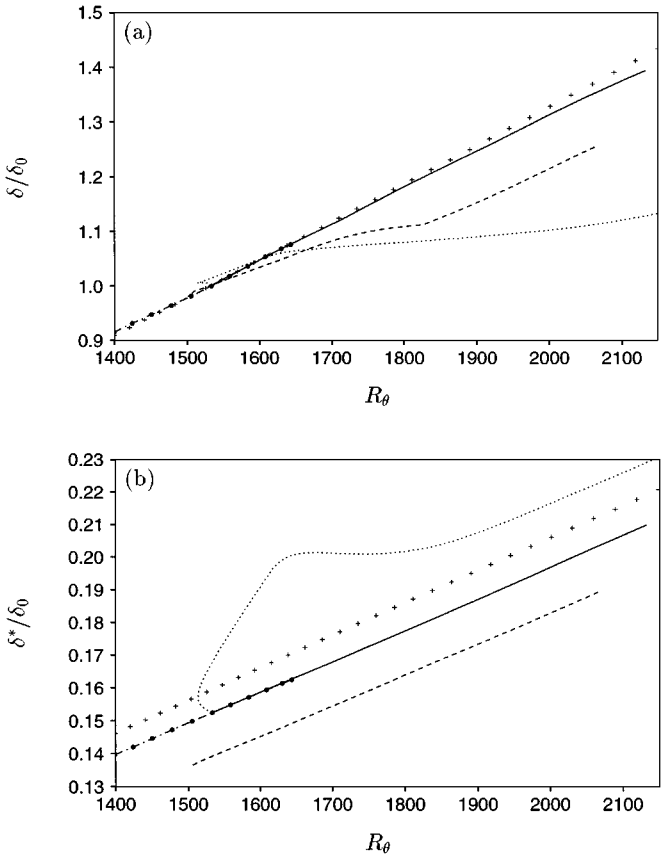

FIG. 2. Evolution of the boundary layer thickness in the inflow–outflow simulations: (a), 99% velocity thickness; (b) displacement thickness: ———, simulation using the modified Spalart method inflow; – – –, simulation using the parallel-flow method inflow; · · ·, simulation using the random fluctuation method inflow; •-•, results of the inflow calculation using the modified Spalart method; +, momentum integral estimate.

The behavior near the inlet ($R_\theta = 1530$) is also unusual, where the curve begins on a leftward trajectory, then doubles back and moves to the right. This anomaly is caused by an initial drop in the momentum thickness, which enters the plot through the abscissa. Since the momentum thickness Reynolds number is used to scale several of the subsequent plots, similar behavior will be noted in those as well.

The evolution of the displacement thickness is shown in Fig. 2b. Once again the results from the modified Spalart method simulation and its inflow–outflow counterpart are nearly indistinguishable in the region of overlap. There is also no change in behavior with increasing downstream distance and the results are in good agreement with the momentum integral estimate. In terms of the evolution of the displacement thickness, the parallel-flow boundary layer appears to produce acceptable inflow data. However, the actual values of the ratio of displacement to boundary layer thickness from this method do not agree as well with the momentum integral estimate. The random fluctuation method produces a large transient, but the correct slope is more or less achieved by the domain exit.

Figure 3 shows the evolution of the momentum thickness. As with the boundary layer and displacement thicknesses, the modified Spalart simulation and its inflow–outflow

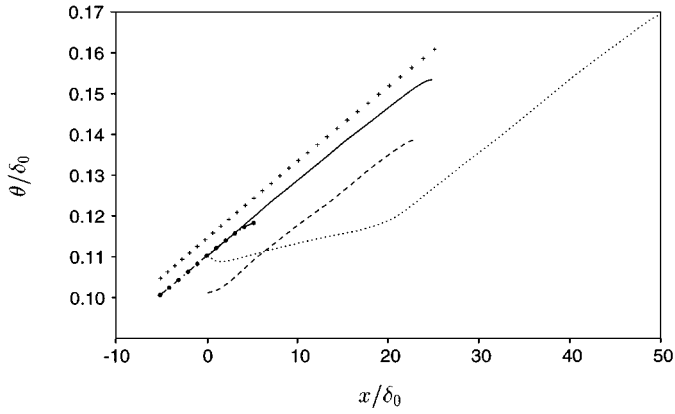

FIG. 3. Evolution of the momentum thickness in the inflow–outflow simulations: ———, simulation using the modified Spalart method inflow; - - -, simulation using the parallel-flow method inflow; · · ·, simulation using the random fluctuation method inflow; •·•, results of the inflow calculation using the modified Spalart method; +, momentum integral estimate.

counterpart agree quite well over most of the overlap region. The small deviation near the exit of the inflow calculation is due to errors produced by the exit boundary condition. (A similar decrease in slope can be seen near the end of the main simulation.) This feature illustrates why it is necessary to displace the recycle station slightly upstream of the exit boundary in the inflow generation simulation. Aside from this small deviation, the momentum thickness evolution shows no sign of readjustment with downstream distance. Aside from a small transient near the inlet, the parallel-flow method yields a momentum thickness evolution that is acceptable. However, as with the other thickness parameters, the momentum thickness is shifted from its expected value, in this case being about 10% low. The random fluctuation method again produces poor results. The initial growth rate is almost a factor of 4 too small. Once the flow "transitions," the growth rate is greatly improved and is comparable to the other curves. The initial slow evolution of the momentum thickness required that the computational domain be longer for the simulation using random fluctuation inflow as compared with the other two. This is evident in Fig. 3, where the simulation with inflow generated using the random fluctuation method is carried downstream nearly 50 initial boundary layer thicknesses. This feature underscores the two compelling disadvantage of the random fluctuation approach: (1) a lengthy development section must be included to allow realistic turbulence to develop and (2) it is very hard to anticipate what values of the integral thicknesses will be produced at the end of the development section.

The shape factor (ratio of displacement to momentum thickness) evolution is shown in Fig. 4. Once again the modified Spalart calculation and its corresponding inflow–outflow simulation are in good agreement within the overlap region and no change in behavior is noted downstream. The results are also in very good agreement with the momentum intergral estimate. The results are within 3% of the shape factor from Spalart's [1] calculation (solid triangle) and within 4% of the experimental measurement due to Purtell *et al.* [25] (solid square). When the parallel-flow method is used, the shape factor is a few percent low at the inlet, but this error diminishes with increasing streamwise distance. The results from the random fluctuation method are again quite poor. The shape factor increases initially

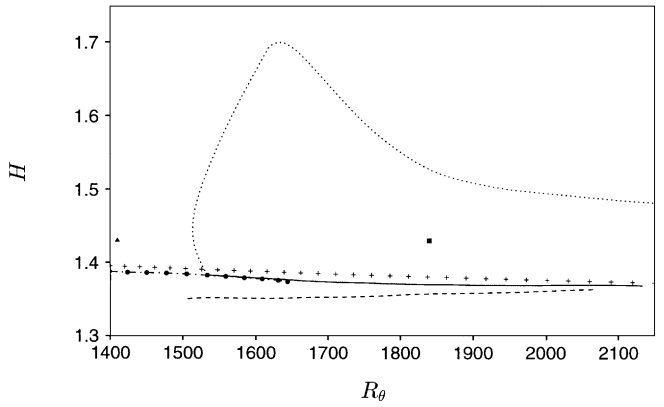

FIG. 4. Evolution of the shape factor in the inflow–outflow simulations: ———, simulation using the modified Spalart method inflow; - - -, simulation using the parallel-flow method inflow; · · ·, simulation using the random fluctuation method inflow; •-•, results of the inflow calculation using the modified Spalart method; ▲, Spalart [1]; ■, Purtell *et al.* [25]; +, momentum integral estimate.

toward the laminar value of 2.6; then following "transition" it relaxes back toward more reasonable values for a turbulent boundary layer. Note, however, that the 50 boundary layer thicknesses of spatial evolution are not sufficient to produce a canonical turbulent boundary layer when this method is used.

Figure 5 shows the computed skin friction. Once again the results from the modified Spalart simulation and its inflow–outflow counterpart are in good agreement within the region of overlap and no significant adjustment takes place downstream. They are in reasonable agreement with the momentum integral estimate. The results are within 2% of the computations of Spalart [1] (solid triangle) and within 4% of the experimental data of Murlis *et al.* [26] (solid diamond). The parallel-flow method produces a small initial transient, followed by an acceptable skin friction evolution. The random fluctuation method exhibits a

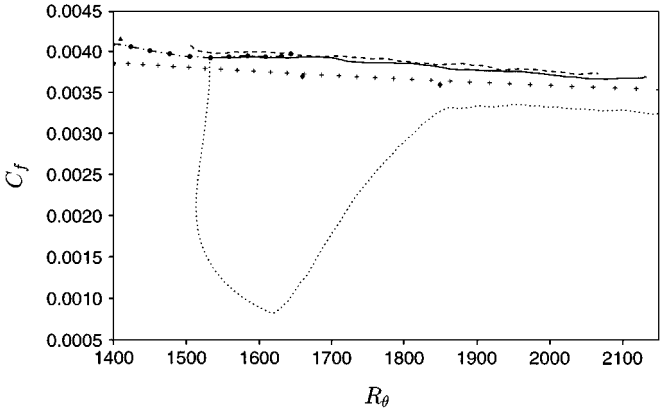

FIG. 5. Evolution of the skin friction in the inflow–outflow simulations: ———, simulation using the modified Spalart method inflow; - - -, simulation using the parallel-flow method inflow; · · ·, simulation using the random fluctuation method inflow; •-•, results of the inflow calculation using the modified Spalart method; ▲, Spalart [1]; ◆, Murlis *et al.* [26]; +, momentum integral estimate.

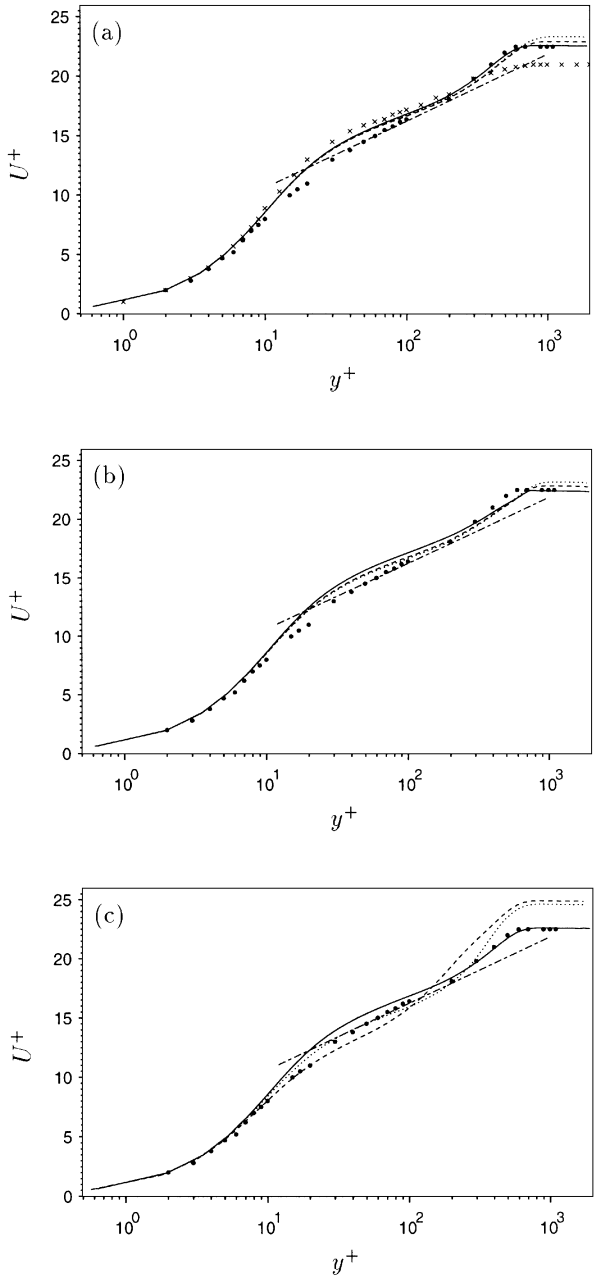

FIG. 6. Mean velocity profiles from the inflow–outflow simulations: (a), simulation using the modified Spalart method inflow; (b), simulation using the parallel-flow method inflow; (c), simulation using the random fluctuation method inflow: ———, $R_\theta = 1530$; - - -, $R_\theta = 1850$; $\cdots$, $R_\theta = 2050$; •, Spalart [1], $R_\theta = 1410$; ×, Rai and Moin [3], $R_\theta = 1350$; – – –, $2.44 \ln y^+ + 5.2$.

sharp drop in skin friction followed by an increase once the flow develops realistic turbulent structure.

Mean velocity profiles for three streamwise locations are shown in Fig. 6. The first station is chosen to be inflow plane, which is effectively the result of the modified Spalart method. This arrangement allows us to compare the results of the modified Spalart method with

Spalart's [1] original computations. It also makes the differences in behavior more apparent as the flow evolves downstream.

The simulation with inflow obtained using the modified Spalart method (Fig. 6a) yields canonical mean profiles as the flow evolves downstream. In particular, the viscous sublayer and logarithmic region are largely unchanged when plotted in wall units, while the expected Reynolds number dependence is displayed in the wake region. The results also agree well with Spalart [1], except in the logarithmic region where the mean velocity is slightly overpredicted. This defect is a common feature of simulations using finite-difference methods on relatively coarse meshes and is not related to the rescaling approach used in the inflow generation process. In support of this claim, note that the results of Rai and Moin [3] (crosses) contain a similar discrepancy that is actually slightly worse than in our calculation. It is also important to note that the shape of the velocity profile shows no tendency to change with increasing streamwise distance in the inflow–outflow simulation. The velocity overshoot has also been observed by Cabot [27] and Lund and Kaltenbach [28] in finite difference calculations of turbulent channel flow. As shown in both of these works, the overshoot can be reduced through mesh refinement. In order to confirm this trend in the present study, we performed an additional simulation using 25% more points in the streamwise direction and 50% more in the wall-normal direction. This simulation did indeed yield a slight improvement to the logarithmic layer.

The simulation with the parallel-flow method (Fig. 6b) produces a small transient, where the initial profile shape changes in the logarithmic and wake regions. The parallel-flow method produces a profile that has a larger deviation in the logarithmic region. This discrepancy diminishes with increasing streamwise distance and the profiles at the last two stations collapse in the logarithmic region. These latter two profiles are also nearly identical to the corresponding pair in the case with the modified Spalart method inflow (Fig. 6a). More detailed measurements indicate that the transient is no longer visible in the mean velocity profile beyond about 10 boundary layer thicknesses downstream of the inlet.

The random fluctuation method (Fig. 6c) leads to rather anomalous behavior where the profile experiences a large transient as it evolves downstream. At the second plotting station, the mean velocity is underpredicted in the logarithmic region and an unusually large wake develops. The profile then starts to relax back to the expected shape with an increase of the velocity in the logarithmic region and a reduction in the wake. The apparent agreement with the standard logarithmic law (between $y^+ = 30$ and 60) for the third plotting station is fortuitous; profiles further downstream show an overprediction in this region similar to that in the other two simulations. Consistent with this observation is the fact that the profiles do not reach a self-similar state by the domain exit, although it is roughly 50 initial boundary layer thicknesses downstream of the inlet.

Figure 7 shows velocity fluctuation and shear stress profiles for three streamwise locations. The modified Spalart method (solid curve in Fig. 7a) produces results that are in good agreement with the original calculations of Spalart. The only significant deviation is an overprediction of the peak streamwise fluctuation (u') and an underprediction of the spanwise fluctuation (w'). This defect is similar to the velocity overshoot in the mean velocity profile in that it is related to the numerical method and not to the rescaling procedure. In support of this, note that a similar problem exists for the data of Rai and Moin [3] and that the trend persists throughout our entire inflow–outflow calculation. Note that the profiles do not collapse perfectly for the three Reynolds numbers. Part of this is due to the scaling used

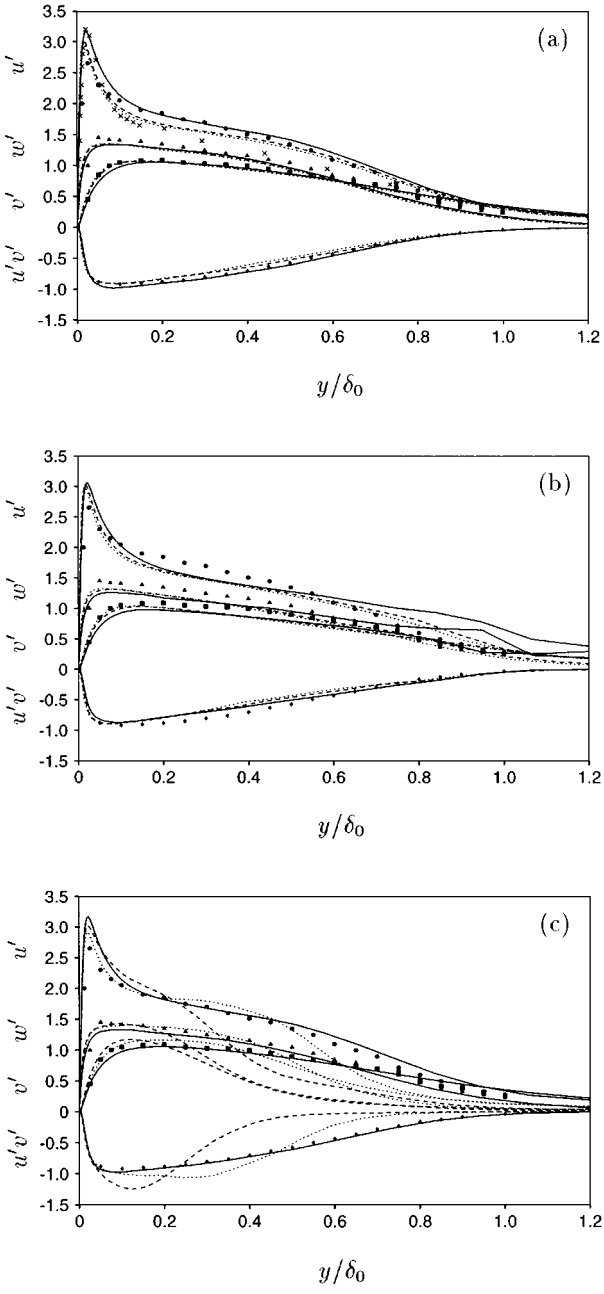

FIG. 7. Velocity fluctuation and shear stress profiles (scaled in wall units) from the inflow–outflow simulations: (a), simulation using the modified Spalart method inflow; (b), simulation using the parallel-flow method inflow; (c), simulation using the random fluctuation method inflow: ———, $R_\theta = 1530$; - - -, $R_\theta = 1850$; · · ·, $R_\theta = 2050$; filled symbols are the data from the simulations of Spalart [1] at $R_\theta = 1410$; ×, Rai and Moin [3], $R_\theta = 1350$.

and part is due to a small adjustment as the flow evolves downstream. The chosen scaling should collapse the profiles better in the outer region opposed to the near wall region and this is seen to be the case. If the profiles are plotted against y^+, an improved collapse is obtained in the near-wall region. Using inner scalings, the two downstream profiles collapse

perfectly out to about $y^+ = 300$, while the profiles from the inlet station remain slightly displaced from the other two, especially for u' and uv. This behavior indicates that a small adjustment takes place between the fluctuations in the inflow generation simulation and the spatially evolving case. It is interesting to note that the streamwise fluctuations and shear stress from the inflow plane agree best with Spalart [1]. It is possible that the rescaling method common to both approaches results in slightly higher values of these quantities.

Simulations performed using the parallel-flow inflow (Fig. 7b) results in profiles that yield an acceptable degree of collapse. The largest discrepancy occurs in the outer region of the streamwise and spanwise profiles where the values from the first station are too large. This is a side effect of the boundary conditions used in the inflow generation simulation. When the parallel-flow method is used, the boundary layer edge is rigidly defined as the position where the no stress, zero normal velocity boundary conditions are applied. This condition forces v' to vanish at the boundary layer edge and results in a redistribution of the wall-normal fluctuation energy into u' and w'. Another side effect of this approach is that there are no naturally occurring fluctuations in the region between the boundary layer edge and the upper boundary of the computational domain at the inflow plane. In an attempt to remedy this, random fluctuations were superimposed on the free-stream velocity in this region. The scaling of these disturbances is rather arbitrary, and in this case, the isotropic distribution $u_i' = 0.1U_\infty \exp[-2(y/\delta - 1)]$ was used. The high-frequency random disturbances decay rapidly and after a few boundary layer thicknesses of spatial evolution, roughly the correct level of free-stream fluctuations are obtained. Aside from the problems near the boundary layer edge, the remainder of the profiles collapse reasonably well and are in acceptable agreement with Spalart [1]. When plotted against y^+, the collapse is improved in the near wall region. Once again the profiles from the second two stations collapse almost perfectly, whereas the data from the first remain slightly displaced. Thus there is also a small readjustment of the fluctuations when the parallel-flow method is used.

As in the case of the mean velocity profile, the results from the simulation using the random fluctuation method (Fig. 7c) are poor. The initially correct fluctuation profiles decay in the outer region. With increasing streamwise distance, the fluctuations and shear stress rebuild in this region, but the process is not nearly complete by the third plotting station which is roughly 35 initial boundary layer thicknesses downstream of the inlet.

6. SUMMARY AND CONCLUSIONS

A straightforward method for generating physically realistic turbulent inflow data for simulations of spatially developing boundary layers has been presented. The approach is based on extracting time-dependent velocity data from an auxiliary simulation of a flat plate boundary layer. The latter is achieved through a simplification of the method developed by Spalart and Leonard [2] and Spalart [1] for simulation of boundary layers in periodic domains. Our approach is to "recycle" the turbulent velocity field from a station near the domain exit and reintroduce it as the inflow boundary condition. The end result is a straightforward spatially evolving simulation that generates its own inflow conditions. This approach has the advantage that an existing inflow–outflow code can be converted to an inflow generation device through the addition of one simple subroutine. The method was shown to produce results that agree quite well with the original calculations of Spalart [1].

The modified Spalart method was also used to generate inflow data for an inflow–outflow large eddy simulation of a flat-plate boundary layer. For comparison, simulations were also

performed using two simpler methods of inflow generation: data taken from a parallel-flow boundary layer calculation and synthetic turbulence generated by a random number scheme. The modified Spalart method consistently produced the most accurate inflow data with little or no transient near the inlet boundary. This fact implies that the method can be used without need for a development section. The method also gives direct control of the skin friction and momentum thickness and thus these quantities can be set to the desired values at the inflow boundary.

The parallel-flow method resulted in a modest transient followed by a general recovery in most quantities within 10 boundary layer thicknesses of spatial evolution. The method also produced somewhat inaccurate boundary layer thickness and shape factor parameters. While the parallel-flow method used in conjunction with a development section may be acceptable for some situations, the cost of generating inflow data is similar to the modified Spalart method. Since the addition of a development section will increase the overall cost of the simulation and reduce the ability to control the boundary layer characteristics at its end, we do not see any reason to use this method in place of the modified Spalart method.

The random fluctuation method was found to result in a rather poor inlet condition. The synthetic velocity field lacks both turbulent structure and nonlinear energy transfer. We found that a development section of up to 50 boundary layer thicknesses is needed to produce realistic turbulence and that the integral thicknesses and skin friction evolve to rather nonstandard values over this distance. It should be mentioned that while more sophisticated random fluctuation methods exist, the use of these probably does not improve the situation much. None of the methods can produce realistic turbulent structure and a development section will always be required in order to produce them. As an example, Le and Moin [5, 6] used an improved method where the spectrum of the velocity fluctuations was prescribed realistically in both space and time. Aside from the need to specify the frequency and wavenumber spectra, this procedure also requires additional computational effort to evaluate fast Fourier transforms. The computational grid was also very fine (DNS) which seems aid in the development of turbulence from the random starting condition [7, 8]. Despite these things, their computed skin friction still exhibited a large transient in the development section, dropping by more than 70% before recovering to within 10% of the target value at the step corner (10 boundary layer thicknesses downstream of the inlet). Although acceptable results were obtained for the flow downstream, it could be that the large distortion caused by the separation limits the sensitivity to the precise details of the incoming boundary layer in this flow. It is not clear whether inflow conditions with such large residual errors would be sufficient in the general case. In any event, there appears to be little motivation to continue working with random fluctuation methods in light of the availability of more accurate approaches.

While our choice of a flat plate as an inflow–outflow test case may seem overly simplified, there is considerable additional evidence that the conclusions drawn here are more generally applicable. As described in Section 5 a flat plate was used in this work in order to verify that the modified Spalart method produces a natural equilibrium boundary layer. Errors in the rescaling procedure, as well as contamination from the exit boundary condition, could lead to nonequilibrium effects in the inflow data which would show up as an adjustment in the boundary layer growth as it evolves downstream in the inflow–outflow simulation. Such changes would not be visible in a more complicated flow due to the presence of pressure gradients and/or geometrical changes. More challenging test cases have been performed, however, and the consistent indication is that the modified Spalart method continues to be

a means for producing an accurate inflow condition for more complicated flows. Lund and Moin [11] used both the parallel-flow and modified Spalart methods to generate inflow for their simulation of a boundary layer on a concave surface. They found that the modified Spalart method produced the most accurate inflow condition. Wu and Squires [29] used the method to generate inflow data for a boundary layer that encounters a bump. They obtained good agreement with experimental data without need for a development section. Finally, Wang and Moin [30] used the method for their simulation of the aft section of a hydrofoil. Once again, good agreement with experimental data was obtained without need for a development section.

Another, perhaps surprising, result of our study is that the modified Spalart method will probably result in the lowest overall cost when the expense of a development section is considered. While the supposed main motivation for using the random fluctuation method is its simplicity and extreme computational efficiency, a development section of at least 20 boundary layer thicknesses is required. This distance is double the extent of the domain used in our modified Spalart simulation, and thus, the latter method used without a development section will cut in half the overhead for generating the inflow data. It is possible to lower the overhead further by taking advantage of the fact that the inflow generation code can make use of a regular cartesian grid and a direct solver for the pressure Poisson equation (for incompressible flow). Our experience is that such a simplified code runs at least 4 times faster on a per mesh point per time step basis, as compared with a complex geometry code that would normally be used for the main simulation. Thus, if a dedicated code is used for the inflow generation, a cost savings of up to a factor of 8 can be realized when our method is compared with the random fluctuation method used in conjunction with a development section. The cost for generating inflow data with the parallel-flow method is similar to that of the modified Spalart method, but the inclusion of a development section will result in higher overall cost.

Finally we should mention that while our method appears to be rather accurate and efficient, there are a few potential enhancements that may serve to increase its utility further. The first of these is to merge the inflow generation procedure with the main simulation by simply recycling the velocity field taken a short distance downstream of the inlet in the main simulation. This procedure has the advantage that it avoids an auxiliary simulation and effectively eliminates the influence of the outflow boundary condition errors on the velocity field at the recycle station. In order to utilize this approach, however, the boundary layer must not be acted on by significant pressure gradients or geometrical changes between the inlet and recycle station. In effect this requirement may dictate that the simulation begin further upstream, which will reduce some of the benefit of this approach. Another technical detail is that it would be wasteful to subject the entire simulation domain to the "development time" during which a realistic inflow condition evolves out of an arbitrary starting condition. Thus, one should really achieve a stationary state by running a modified Spalart simulation on a limited domain first before switching over to the integrated inflow procedure.

The second potential enhancement is to account for the effects of a pressure gradient in the inflow condition. Doing this may avoid the necessity of displacing the inlet boundary upstream to a position where the pressure gradient is minimal. For cases in which severe or extended pressure gradients exist near the inlet boundary, the modified Spalart method can be extended to allow for a restricted class of equilibrium boundary layers that develop under power-law pressure gradients [31]. While equilibrium pressure distributions may not be that common in practice, they certainly can be used as a first approximation.

Assuming an equilibrium pressure distribution, the same scaling laws described in Section 3 continue to apply and the required changes involve only the computation of the friction velocity at the inlet and the vertical velocity distribution at the upper boundary. The Ludwig–Tillmann [14] correlation applied between the rescale and inlet location is used to obtain the friction velocity at the inlet. The vertical velocity at the upper boundary is determined from the integrated continuity relation, $v(x) = U_e d\delta^*/dx + (\delta^* - h) dU_e/dx$, where U_e is the local boundary layer edge velocity. Although extensive tests of simulations with pressure gradients have not been performed, the preliminary conclusion from a few isolated test cases is that the procedure continues to produce accurate inflow data under these circumstances.

APPENDIX

A. *Random Fluctuation Inflow Generation Method*

The random fluctuation method is designed to match a prescribed mean flow and Reynolds stress tensor. Let the target mean flow profile be denoted by $U(y), V(y)$, and the target Reynolds stress tensor by $R_{ij}(y) = \langle u_i u_j \rangle_{z,t}$, where u_i is the velocity fluctuation (i.e., $\langle u_i \rangle_{z,t} = 0$). The operation $\langle\ \rangle_{z,t}$ is an average over the spanwise direction and time. At each time step in the simulation, inflow data are generated in a loop running over the y direction. For each y location, the following sequence of operations is peformed:

1. Three sequences of random numbers $\tilde{u}(z), \tilde{v}(z), \tilde{w}(z)$, are generated. They are conditioned so that each distribution has zero mean, unit variance, and zero covariance with the other two distributions (i.e., $\langle \tilde{u}_i \tilde{u}_i \rangle_z = 0$ for $i \neq j$).
2. The velocity field is then constructed according to

$$u_i(y, z) = U_i(y) + a_{ij} \tilde{u}_j(z), \tag{26}$$

where the elements of the amplitude tensor a_{ij} are related to the Reynolds stress tensor via

$$\begin{aligned} a_{11} &= \sqrt{R_{11}}, \\ a_{21} &= R_{21}/a_{11}, \\ a_{22} &= \sqrt{R_{22} - a_{21}^2}, \\ a_{31} &= R_{31}/a_{11}, \\ a_{32} &= (R_{32} - a_{21}a_{31})/a_{22}, \\ a_{33} &= \sqrt{R_{33} - a_{31}^2 - a_{32}^2}. \end{aligned} \tag{27}$$

All elements of a_{ij} not listed above are zero.

Our procedure makes use of random numbers that are de-correlated in both space and time. The basic procedure can be modified to allow for nonzero correlations through the use of a fast Fourier transform in space and/or time. In this case, the spectrum of the fluctuations is prescribed in Fourier space and an inverse transform provides the velocity fluctuation distribution. Le and Moin [5, 6] used this procedure to generate inflow conditions for a backward-facing step. The behavior of the method is much the same as in our simplified approach, however, and we have not gone to the extra effort to implement this strategy.

B. *Parallel-Flow Inflow Generation Method*

The parallel-flow boundary layer simulation is very similar to a turbulent channel flow calculation. Periodic boundary conditions are used in the streamwise and spanwise directions and the flow is driven by a constant streamwise body force (uniform pressure gradient). The only difference with a channel flow calculation is that the no slip conditions at the upper wall are replaced by the following symmetry conditions:

$$\frac{\partial u}{\partial y} = 0, \quad v = 0, \quad \frac{\partial w}{\partial y} = 0. \tag{28}$$

For a laminar flow, the procedure would simply produce the lower half of a channel flow profile. In a turbulent flow, the symmetry conditions also produce something like half of a channel flow, which can be used as a rough approximation to a turbulent boundary layer.

C. *Momentum Integral Analysis*

The momentum integral estimates used in this work can be found in White [32]. The relevant formulas are repeated here for convenience. For the purpose of the estimates, the mean velocity profile is assumed to obey the law of the wake [24] over the entire extent of the layer:

$$U^+ = \frac{1}{\kappa}\ln(y^+) + B + \frac{2\Pi}{\kappa}\sin^2\left(\frac{\pi}{2}\eta\right), \tag{29}$$

where $U^+ = U/u_\tau$, $y^+ = yu_\tau/\nu$, $\eta = y/\delta$, κ, B, are constants, and Π is a parameter that depends on the pressure gradient. The boundary layer edge, δ, is defined as the position where $U = U_\infty$. Making use of this condition, the above relation implies

$$R_\delta \equiv \frac{U_\infty \delta}{\nu} = \lambda \exp[\kappa(\lambda - B) - 2\Pi], \tag{30}$$

where λ is the wall friction parameter:

$$\lambda \equiv \frac{U_\infty}{u_\tau} = \sqrt{\frac{2}{C_f}}. \tag{31}$$

The above two relations are used to rewrite (29) as

$$\frac{U}{U_\infty} = 1 + \frac{1}{\kappa\lambda}\left\{\ln(\eta) + 2\Pi\left[\sin^2\left(\frac{\pi}{2}\eta\right) - 1\right]\right\}. \tag{32}$$

This relation can be integrated to yield the displacement and momentum thicknesses. The end results are

$$R_{\delta^*} = \left(\frac{1+\Pi}{\kappa\lambda}\right) R_\delta, \tag{33}$$

$$R_\theta = \left\{\frac{1+\Pi}{\kappa\lambda} - \frac{1}{\kappa^2\lambda^2}\left[2 + 2\Pi\left(\frac{\mathrm{Si}(\pi)}{\pi} + 1\right) + \frac{3}{2}\Pi^2\right]\right\} R_\delta, \tag{34}$$

where $\mathrm{Si}(\pi) \simeq 1.852$ is the sine integral evaluated at π.

The streamwise distance is determined by integrating the relation

$$2\frac{dR_\theta}{dR_x} = C_f \tag{35}$$

while using (31) to yield

$$R_x - R_{x0} = \int_{\lambda_0}^{\lambda} \lambda^2 \frac{dR_\theta}{d\lambda} d\lambda, \tag{36}$$

where the subscript 0 refers to reference position (taken to be the inlet of the inflow–outflow simulations).

Note that (30), (33), (34), and (36) contain the wall shear parameter, λ, as an independent variable. Results are generated by stepping through values of λ and then rearranging the outputs to yield the various quantities as functions of either R_θ or R_x. The constants were set as follows: $\kappa = 0.41$, $B = 5.0$, and $\Pi = 0.5$.

ACKNOWLEDGMENTS

Financial support for this work was provided from the Office of Naval Research and Air Force Office of Scientific Research. TSL acknowledges support from ONR Grant N-00014-91-J-4072 (Program Officer: Dr. L. Patrick Purtell) and AFOSR Grant F49620-92-J0003 (Program Officer: Dr. James McMichael). XW and KDS acknowledge support under ONR Grants N-00014-94-1-0047 and N-00014-94-1-1053 (Program Officer: Dr. L. Patrick Purtell).

REFERENCES

1. P. R. Spalart, Direct simulation of a turbulent boundary layer up to $Re_\theta = 1410$, *J. Fluid Mech.* **187**, 61 (1988).
2. P. R. Spalart and A. Leonard, Direct numerical simulation of equilibrium turbulent boundary layers, in *Proc. 5th Symp. on Turbulent Shear Flows, Ithaca, NY, 1985*.
3. M. M. Rai and P. Moin, Direct numerical simulation of transition and turbulence in a spatially evolving boundary layer, *J. Comput. Phys.* **109**, 169 (1993).
4. S. Lee, S. K. Lele, and P. Moin, Simulation of spatially evolving turbulence and the applicability of Taylor's hypothesis in compressible flow, *Phys. Fluids A* **4**, 1521 (1992).
5. H. Le and P. Moin, *Direct Numerical Simulation of Turbulent Flow over a Backward-Facing Step*, Report TF-58, Thermosciences Div., Dept. Mech. Eng., Stanford University, Stanford, CA 94305, 1994.
6. H. Le, P. Moin, and J. Kim, Direct numerical simulation of turbulent flow over a backward-facing step, *J. Fluid Mech.* **330**, 349 (1997). [Thermoscience Div., Dept. Mech. Eng., Stanford University]
7. K. Akselvoll and P. Moin, Application of the dynamic localization model to large eddy simulation of turbulent flow over a backward-facing step, in *Engineering Applications to Large Eddy Simulation*, edited by U. Piomelli and S. Ragab (ASME, New York, 1993).
8. K. Akselvoll and P. Moin, *Large Eddy Simulation of Turbulent Confined Coannular Jets and Turbulent Flow over a Backward Facing Step*, Report TF-63, Thermosciences Div., Dept. Mech. Eng., Stanford University, Stanford, CA 94305, 1995.
9. H.-J. Kaltenbach, Large eddy simulation of flow in a plane, asymmetric diffuser, Annual Research Briefs—1993, Center for Turbulence Research, 101 (1993).
10. T. S. Lund, Large eddy simulation of a boundary layer with concave streamwise curvature, Annual Research Briefs—1993, Center for Turbulence Research, 91 (1993).
11. T. S. Lund and P. Moin, Large eddy simulation of a concave wall boundary layer, *Int. J. Heat Fluid Flow* **17**, 290 (1996).

12. Y. Na and P. Moin, *Direct Numerical Simulation of Turbulent Boundary Layers with Adverse Pressure Gradient and Separation*, Report TF-69, Thermosciences Div., Dept. Mech. Eng., Stanford University, Stanford, CA 94305, 1996.
13. P. R. Spalart and H. W. Watmuff, Experimental and numerical study of a turbulent boundary layer with pressure gradients, *J. Fluid Mech.* **249**, 337 (1993).
14. H. Ludwig and W. Tillmann, Untersuchungen uber die wandschubspannung turbulenter reibungsschichten, *Ing.-Arch.* **17**, 288 (1949). [Transl. as NACA *Tech. Memo 1285*, 1949]
15. M. Germano, U. Piomelli, P. Moin, and W. H. Cabot, A dynamic subgrid-scale eddy viscosity model, *Phys. Fluids A* **3**, 1760 (1991).
16. D. K. Lilly, A proposed modification of the Germano subgrid-scale closure method, *Phys. Fluids A* **4**, 633 (1992).
17. S. Ghosal, T. S. Lund, P. Moin, and K. Akselvoll, A dynamic localization model for large-eddy simulation of turbulent flows, *J. Fluid Mech.* **286**, 229 (1995).
18. C. Meneveau, T. S. Lund, and W. Cabot, A Lagrangian dynamic subgrid-scale model of turbulence, *J. Fluid Mech.* **319**, 353 (1996).
19. A. J. Chorin, A numerical method for solving incompressible viscous flow problems, *J. Comput. Phys.* **2**, 745 (1967).
20. J. Kim and P. Moin, Application of a fractional-step method to incompressible Navier–Stokes equations, *J. Comput. Phys.* **59**, 308 (1985).
21. F. H. Harlow and J. E. Welch, Numerical calculation of time-dependent viscous incompressible flow of fluid with free surface, *Phys. Fluids* **8**, 2182 (1965).
22. T. Y. Han, J. C. S. Meng, and G. E. Innis, An open boundary condition for incompressible stratified flows, *J. Comput. Phys.* **49**, 276 (1983).
23. D. B. Spalding, A single formula for the law of the wall, *J. Appl. Mech.* **28**, 455 (1961).
24. D. E. Coles, The law of the wake in a turbulent boundary layer, *J. Fluid Mech.* **1**, 191 (1956).
25. L. P. Purtell, P. S. Klebanoff, and F. T. Buckley, Turbulent boundary layers at low Reynolds numbers, *Phys. Fluids A* **24**, 802 (1981).
26. J. Murlis, H. M. Tsai, and P. Bradshaw, The structure of turbulent boundary layers at low Reynolds number, *J. Fluid Mech.* **122**, 13 (1982).
27. W. H. Cabot, Local dynamic subgrid-scale models in channel flow, Annual Research Briefs—1994, Center for Turbulence Research, 143 (1994).
28. T. S. Lund and H.-J. Kaltenbach, Experiments with explicit filtering LES using a finite difference method, Annual Research Briefs—1995, Center for Turbulence Research, 91 (1995).
29. X. Wu and K. D. Squires, Numerical investigations of the turbulent boundary layer over a bump, *J. Fluid Mech.*, in press.
30. M. Wang and P. Moin, private communication, 1997.
31. H.-J. Kaltenbach, private communication, 1995.
32. F. M. White, *Viscous Fluid Flow* (McGraw–Hill, New York, 1974).